Two-stage Battery Energy Storage Power Conversion System Based on Dual Active Bridge

Liangyi Wang[1], Ning Gao[1*]and Weimin Wu[1]
1 Department of Electrical Engineering, Shanghai Maritime University, Shanghai, China
*E-mail: ngao@shmtu.edu.cn

***Abstract*- In this paper, the basic principle and control strategy of a 110V/3kW two-stage dual-active-bridge-based battery energy storage power conversion system are introduced. The parameter design of its control loop is provided in detail. Meanwhile, a small-signal impedance model of power conversion system is established to analyze the stability under the condition of weak grid. In the end, the simulation and experimental results are given to confirm the feasibility of designed control loop and the correctness of proposed impedance model.**

***Keywords*— Battery energy storage power conversion system, Dual active bridge, Small-signal impedance model, Weak grid stability**

I. INTRODUCTION

At present, the environmental pollution and energy crisis caused by traditional fossil fuels are being increasingly serious, clean energy represented by solar and wind energy has attracted more and more scholars' attention. However, the volatility and intermittency of these new energy cause negative impacts when they are applied to grid-connected systems. Battery energy storage system (BESS) is usually adopted in this situation to improve the system performance [1].

Traditional power frequency transformers are often used as the electrical isolation and voltage matching unit between the grid and energy storage equipment [2]. However, with the growing popularity of microgrids and mobile energy storage power stations, many new requirements such as flexibility or usability have been put forward for BESS. To meet those demands, BESS integrated with bidirectional isolated dc-dc converter (IBDC) has become the focus of research. Compared with the traditional power frequency transformers, the BESS based on IBDC possesses a smaller volume and can be controlled more flexibly. Meanwhile, the waveform distortion of voltage or current caused by magnetic saturation can be avoided [3]. Therefore, adopting IBDC can improve the energy density of BESS, which has been widely used in the fields of high-power automobiles and photovoltaic systems [4][5].

看看4，5

A typical two-stage battery energy storage power conversion system (BES-PCS) generally consists of two parts: the front-stage DC-DC circuit and the latter-stage DC-AC circuit. The structure of high-frequency isolated DC-DC circuits is various. Among many IBDC topologies, dual active bridge (DAB) has attracted more and more attention in recent years because it is easy to realize soft-switching. The structure of DAB is modular and symmetric which has the capability to transfer power bidirectionally [6]. Although many advanced control methods have been applied to DAB in recent years, the traditional DAB control method, phase shift mode (PSM), is still widely adopted for its advantages: small inertia, strong dynamics and soft-switching control [7]. Besides, as the interface between dc sources and grids, grid-tied inverters also play an important role in BESS. The control strategy for grid-tied inverter should be carefully designed. In recent years, finite control set model predictive control (FCS-MPC) has been widely used for the control of grid-connected inverters. Reference [8] uses virtual flux method together with state observer to carry out FCS-MPC. It proved that full status can be observed without voltage sensors, thus system cost can be greatly reduced. Reference [9] studies a robust FCS-MPC method based on a discrete disturbance observer, which can reduce the inaccuracy caused by parameter mismatch. Although MPC has many advantages, traditional PI control is still worth using in practical engineering applications because of its low computational burden and wide applicability [10].

In recent years, the topology of two-stage BES-PCS has also been studied extensively. Literature [11] calculates the power losses and peak current of a BESS integrated with IBDC. In [12], a multi-level cascaded medium frequency isolated power conversion system is proposed with good performance. Literature [13] addressed a synthetic discrete optimization design method based on advanced components for BESS.

The battery energy storage converter (BESC) is one of the key components in a BESS, which can convert DC power stored in battery into AC power and meet the standard of grid-connection. However, the actual grid can not be simply regarded as an ideal voltage source, which usually includes a certain inductance. When BESC is connected to a weak grid, the system may become unstable. Therefore, it is of great practical significance to establish the impedance model of the BESC to analyze and predict its operation stability when it is connected to a weak grid. Reference [14] uses harmonic linearization and Fourier analysis techniques to describe the impedance mapping model, the mapping process of currents and voltages in switching circuit is also analyzed.

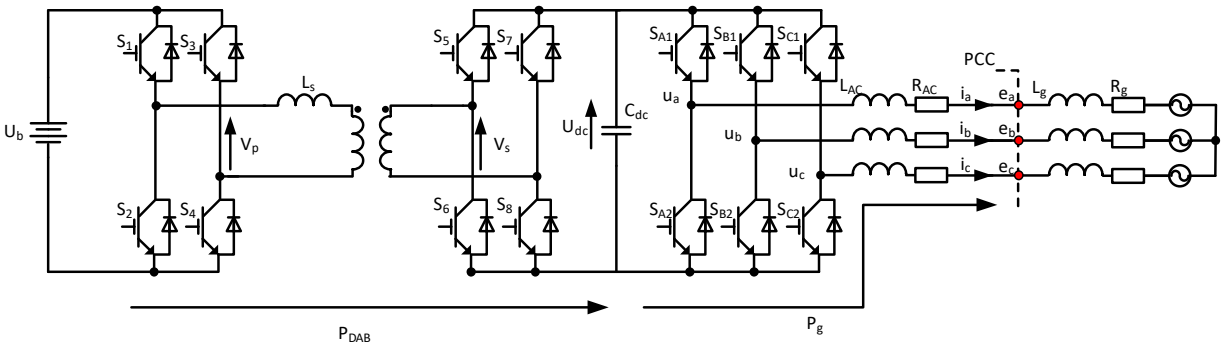

Fig. 1. Circuit configuration of the two-stage BES-PCS based on DAB

Reference [15] proposed a different approach to analyze the instability of synchronization in a VSC system. It can be found that the impedance of grid-tied inverter in d-q frame is similar with negative incremental resistance.

In section II, the mathematical model of a two-stage battery energy storage power conversion system (BES-PCS) based on DAB is constructed. Its control loop is analyzed in section III. Then, in section IV, a small-signal output impedance model of battery energy storage converter is established to analyze the stability under weak grid. Section V gives simulation results to verify the performance of system both in steady and dynamic states, the correctness of impedance model can also be confirmed. Section VI concludes this paper.

II. PRINCPILE OF THE POWER CONVERSION SYSTEM

The Fig. 1 shows the topology of the three closed-loop two-stage BESPCS. A dual active bridge circuit is adopted as the front-stage. Meanwhile, a three-phase inverter bridge circuit is used as the latter-stage. According to the principle of energy conservation, it can be known that the power imbalance between the previous stage and the subsequent stage will directly cause the voltage fluctuation of DC bus, the voltage of DC bus can be denoted as U_{dc}:

$$U_{dc}C\frac{dU_{dc}}{dt} = P_g - P_{DAB} \tag{1}$$

In this paper, the output power of front-stage is regulated by power-closed-loop. Meanwhile, a voltage and current double closed loop is used for the latter-stage. Thus, the DC voltage can be regulated as a constant and the output power factor will be maintained as 1 at the same time.

The front-stage of the converter uses a DAB circuit. The equivalent circuit and parameter definitions are shown in Fig. 1. In Fig. 1, the left side of DAB is the low-voltage side, which is connected to the energy storage battery. The right side is the high-voltage side, which is connected to a capacitor. The DC voltage is converted into an intermediate frequency square wave by two symmetrical H bridges and the power flow is controlled by adjusting the phase shift angle between the primary side and the secondary side of DAB. The transformation ratio of the transformer is 1:1. By adjusting the transformation ratio, the unified access of batteries with different specifications can be met and the standardized modularization of the energy storage converter can be easily realized.

The traditional phase shift mode (PSM) is adopted in the control of DAB. Fig. 2 shows a series of theoretical waveforms of DAB under PSM.

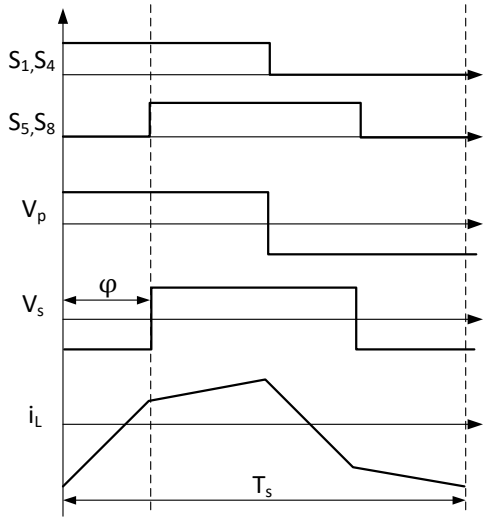

Fig. 2. Theoretical waveforms of DAB under PSM

Under PSM, the primary side and secondary side of DAB respectively generate a set of phase-shifted square waves with the same frequency and a duty cycle of 0.5. The amplitude of the square wave is equal to the voltage of DC bus, and the conduction phases of the square waves on both sides are mutually different. As shown in Fig. 2. When $\varphi>0$, the power flows from the battery to the grid. On the contrary, when $\varphi<0$, the power flows from the grid to the battery. The output power is controlled by adjusting the phase shift angle.

It can be inferred from Fig. 2 that the relationship between output power and phase shift angle is:

$$P_{DAB} = \frac{2}{T_s}\int_0^{T_s/2} U_b i_L(t)dt = \frac{U_b U_{dc}\varphi(\pi - |\varphi|)}{2\pi^2 L_s f_s} \tag{2}$$

From (2), the maximum limit of leakage inductance L_S in the transformer is also derived as:

$$L_s \le \frac{U_b U_{dc}}{8 f_s P_{\max}} \tag{3}$$

The latter-stage adopts a three-phase bridge inverter circuit. In Fig. 1 e_a, e_b and e_c are the instantaneous voltages of grid, i_a, i_b, and i_c represent the grid-side currents; u_a, u_b, and u_c are the output voltage at the midpoint of each bridge; L_{AC} is the inductance of the passive filter and its parasitic resistance is recorded as R_{AC}; Meanwhile, L_g and R_g are the equivalent inductance and resistance on the grid side. u_{dc} is the voltage of DC bus. The mathematical model of the three-phase inverter in abc reference frame can be described as:

$$\begin{cases} L\dfrac{\mathrm{d}i_a}{\mathrm{d}t} + Ri_a = u_a - e_a \\ L\dfrac{\mathrm{d}i_b}{\mathrm{d}t} + Ri_b = u_b - e_b \\ L\dfrac{\mathrm{d}i_c}{\mathrm{d}t} + Ri_c = u_c - e_c \end{cases} \tag{4}$$

In Eq. (4), $L=L_{AC}+L_g$, and $R=R_{AC}+R_g$. after using CLARK transformation and PARK transformation, the mathematical model of the three-phase inverter can be described in the d-q frame:

$$\begin{cases} L\dfrac{\mathrm{d}i_d}{\mathrm{d}t} = -Ri_d + \omega_g L i_q + u_d - e_d \\ L\dfrac{\mathrm{d}i_q}{\mathrm{d}t} = -Ri_q - \omega_g L i_d + u_q - e_q \end{cases} \tag{5}$$

i_q and i_d are the components of the inductor current in q-axis and d-axis respectively. ω_g is the fundamental angular frequency. If the value of i_q is set to 0, the converter can be guaranteed to work with unity power factor.

III. CONTROL STRATEGY

A. *Control Strategy of DAB Power Loop :*

It can be seen from Eq. (1) that the output power of DAB, denoted as P_{DAB}, is equal to the grid-side output power P_g in the steady state. Therefore, both P_{DAB} and P_g can be regulated by controlling the phase shift angle φ. For this reason, a power loop is used in the DC-DC part so that the output power from the DC-DC front stage to the DC-AC rear stage can be regulated as a constant. The specific control strategy is shown in Fig. 3. P_{gref} is the expected grid power. The total output power P_g is obtained through the power calculation module. It is also used as the feedback quantity of power loop. The error between P_g and P_{gref} are the input of PI controller.

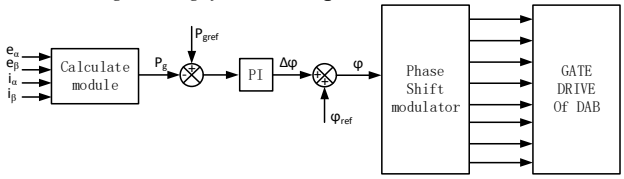

Fig .3. Control Structure of DAB

The error is calculated by a PI controller and $\Delta\varphi$ can be obtained. Meanwhile, φ_{ref} is added as a fed forward, which can improve the dynamic performance of power loop. φ_{ref} can be deduced from Eq. (2)

B. *Control Strategy of DC-AC Side*

The control block diagram of double closed-loop in DC-AC side is shown in Fig 4

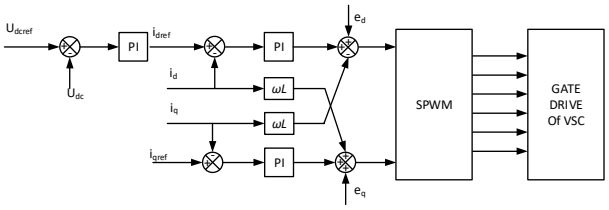

Fig. 4. Control Structure of DC-AC stage

The DC-AC part adopts voltage and current double closed-loop control, including a DC voltage outer loop and an active and reactive current inner loop. The specific control block diagram is shown in Fig. 5. The voltage outer loop takes the voltage of DC bus as the feedback quantity. U_{dcref} is given as the reference. The output of the voltage loop's PI controller, i_{dref}, is used as a reference of the active current inner loop. After transforming the three-phase output currents of the inverter, the currents of i_d and i_q in d-q axis are obtained. After comparing them with the d-q axis reference i_{dref}, i_{qref}, PI control can be executed. By setting the d-axis of the rotating axis in the d-q frame system to coincide with the grid voltage composite vector, and the q-axis given i_{qref} to 0, the power factor of VSC can be set to 1. After the output of the PI regulator is fed forward decoupling, the output voltage u_d*, u_q* are obtained as control commands. Then they are connected to the SPWM module to generate a gate-level drive signal for controlling the IGBTs of VSC after frame transformation.

Fig. 5. Double closed loop control block diagram

C. *Design of PI Parameter for Current Loop:*

Fig. 5 is the control block diagram of the double closed loop. In order to achieve zero-pole cancellation and increase the bandwidth of the current loop, let:

$$\begin{cases} K_{ip} = \dfrac{L}{R} K_{ii} \\ \tau_i = \dfrac{L}{R} \end{cases} \tag{6}$$

According to the block diagram, the open-loop transfer function of the current loop with zero-pole cancellation can be expressed as

$$G_{io}=\frac{\frac{K_{PWM}K_{ip}}{L}}{s\left(1.5T_s s+1\right)} \tag{7}$$

The open loop transfer function of typical I-type system is:

$$G_o=\frac{K_I}{s\left(T_I s+1\right)} \tag{8}$$

Combine Eq. (7) and Eq. (8), we will get:

$$\begin{cases} K_I=\dfrac{K_{PWM}K_{ip}}{L} \\ T=1.5T_s \end{cases} \tag{9}$$

If KT=0.5 and damping ratio is 0.707, it can be considered that the parameters are optimal. When KT is set to 0.5, combining Eq. (6) and Eq. (9), we can get:

$$\begin{cases} K_{ip}=\dfrac{L}{3T_s K_{PWM}} \\ K_{ii}=\dfrac{R}{3T_s K_{PWM}} \end{cases} \tag{10}$$

After comprehensive consideration, the following parameters are selected: K_{ip}=24 , K_{ii}=133.33

D. Design of PI Parameters for Voltage Loop :

The open-loop transfer function of the current loop can be expressed as:

$$G_{ic}=\frac{\frac{K_{PWM}K_{ip}}{sL\left(1.5T_s s+1\right)}}{\frac{K_{PWM}K_{ip}}{sL\left(1.5T_s s+1\right)}+1} \tag{11}$$

In order to simplify the analysis of closed-loop transfer function, the s^2 term can be ignored due to the high switching frequency. As a result, combine Eq. (10) with Eq. (11), the current closed-loop transfer function can be simplified to:

$$G_{ic}=\frac{1}{3T_s s+1} \tag{12}$$

According to the principle of energy conservation, it can be deduced that the current relationship between DC side and grid side is:

$$i_{dc}=0.75mI_m\cos\theta \tag{13}$$

where I_m is the peak value of AC current, m is the modulation ratio. Voltage outer loop is designed with $cos\theta$=1 and m=1.

Assuming that:

$$k_{vi}=\frac{k_{vp}}{\tau_v} \tag{14}$$

Considering the influence of sampling delay on current closed-loop transfer function. The transfer function of voltage loop is as follows:

$$G_{ov}=\frac{\frac{0.75k_{vp}}{\tau_v C_{dc}}\left(\tau_v s+1\right)}{s^2[(3T_s+T_v)s+1]} \tag{15}$$

where T_V is the time constant of voltage sampling, this paper takes $T_V=5T_s$

The open loop transfer function of typical II-type system is:

$$G_o=\frac{K_{II}\left(\tau s+1\right)}{s^2\left(T_{II}s+1\right)} \tag{16}$$

Assuming h as the intermediate bandwidth:

$$h=\frac{\tau_v}{3T_s+T_v} \tag{17}$$

Combine Eq. (15) with Eq. (16) we can get:

$$K_{II}=\frac{0.75k_{vp}}{C_{dc}\tau_v}=\frac{h+1}{2h^2(3T_s+T_v)^2} \tag{18}$$

Combine Eq. (14) with Eq. (18), we can obtain:

$$\begin{cases} k_{vp}=\dfrac{C_{dc}(h+1)}{1.5h(3T_s+T_v)} \\ k_{vi}=\dfrac{C_{dc}(h+1)}{1.5h^2(3T_s+T_v)^2} \end{cases} \tag{19}$$

To meet the control performance required by the voltage loop, h is set to 5. After comprehensive consideration, K_{vp}=6 and K_{vi}=3000 are selected.

IV. IMPEDANCE MODELING

In practice, the grid often contains parasitic inductance, which is a threat to system stability. When the battery energy storage converter is connected to a weak power grid with a large inductive reactance, the system is more likely to become unstable. Therefore, an impedance model of high-frequency isolated two-stage battery energy storage converter is proposed to analyze and predict the operation stability under weak power grid. The stability margin can also be improved by this method.

Based on Norton's theorem, the non-ideal grid can be equivalent to the circuit shown in the Fig. 6. Battery energy storage converter is equivalent to a current source in parallel with its output impedance Z_{out}. The grid is equivalent to a voltage source with grid impedance Z_g in series. $I(s)$ and $U_g(s)$ will not affect the stability of the cascaded system. Only when $Z_g\times Z_{out}^{-1}$ satisfies the generalized Nyquist stability criterion, the stability of grid-connected battery energy storage system can be ensured. Therefore, in order to judge whether the system is stable, it is necessary to establish the impedance model of Z_{out}

To facilitate the solution, the grid inductance is set to 0, which means $Z_g(s)=0$. According to the definition of sequence impedance, $Z_{out}(s)$ can be obtained by calculating the quantitative relationship between $U_g(s)$ and current of PCC, denoted as $I_g(s)$.

Combined with the above analysis, the control block diagram of small signal model for battery energy storage converter in the d-q frame can be represented by Fig. 7.

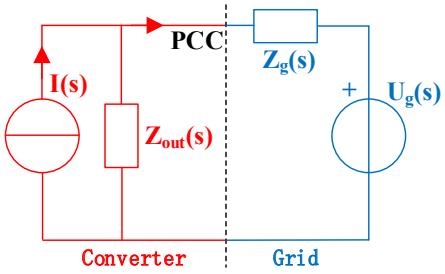

Fig. 6. Equivalent model of battery energy storage converter connected to weak grid

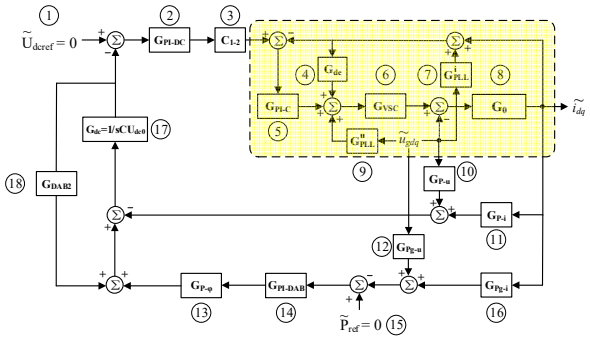

Fig. 7. Control block diagram of small-signal model for battery energy storage converter

In Fig. 7, u_{gdq} and i_{gdq} are the grid voltage and grid current respectively, which can be represented by two 2x1 matrix as follows:

$$\begin{cases} u_{gdq}=\begin{bmatrix} u_{gd} & u_{gq} \end{bmatrix}^T \\ i_{dq}=\begin{bmatrix} i_d & i_q \end{bmatrix}^T \end{cases} \tag{20}$$

For the convenience of explanation, each element in the model is added with its own numerical number, and its meaning will be analyzed one by one below.

1. U_{dcref} is the small-signal disturbance included in the given value of the voltage of DC bus. In steady state, the given value is a constant, which means the disturbance is zero and U_{dcref} is equal to zero.

2. $G_{PI\text{-}DC}$ represents the PI regulator of voltage loop for DC bus, and its mathematical expression is:

$$G_{PI-DC} = k_{vp} + \frac{k_{vi}}{s} \tag{21}$$

3. $C_{1\text{-}2}$ is a custom matrix, its mathematical expression is:

$$C_{1-2} = \begin{bmatrix} 1 & 0 \end{bmatrix}^T \tag{22}$$

4. G_{de} is the cross decoupling matrix required for current closed-loop control in the d-q frame system:

$$G_{de} = \begin{bmatrix} 0 & -\omega L \\ \omega L & 0 \end{bmatrix} \tag{23}$$

5. $G_{PI\text{-}C}$ represents a PI regulator in current loop. Since the variables in d-axis and q-axis need to be controlled, PI regulators of d-axis and q-axis can be written into a matrix, which is shown as follows:

$$G_{PI-C} = \begin{bmatrix} k_{ip}+\frac{k_{ii}}{s} & 0 \\ 0 & k_{ip}+\frac{k_{ii}}{s} \end{bmatrix} \tag{24}$$

6. G_{VSC} is a first-order low-pass element, which is used to characterize the delay characteristics of the subsequent AC-DC converter circuit:

$$G_{VSC} = \frac{1}{T_{s2}s+1} \tag{25}$$

7. G^i_{pll} is the phase-locked loop model 1, which is used to characterize the disturbance included in the output angle of the phase-locked loop caused by the grid voltage disturbance. This disturbance has influence on the calculations of current both in d-axis and q-axis. It can be expressed as:

$$G^i_{pll} = \begin{bmatrix} 0 & I_q \times \dfrac{G_{PI-PLL}}{s+U_{gd}\times G_{PI-PLL}} \\ 0 & -I_d \times \dfrac{G_{PI-PLL}}{s+U_{gd}\times G_{PI-PLL}} \end{bmatrix} \tag{26}$$

where I_d represents the steady-state value of the d-axis current i_d, and I_q represents the steady-state value of the q-axis current i_q. $G_{PI\text{-}PLL}$ stands for a PI regulator in phase-locked loop, and the expression is:

$$G_{PI-PLL} = k_{ppll} + \frac{k_{ipll}}{s} \tag{27}$$

where k_{ppll} and k_{ipll} represent the proportional and integral coefficients of the PI regulator in phase-locked loop, respectively. This expression is the same as $G_{PI\text{-}PLL}$ in Phase Locked Loop Model 2.

8. The model of the filter inductance and its parasitic resistance is represented by G_0, and its expression is:

$$G_0 = \begin{bmatrix} s+\frac{R}{L} & -\omega \\ \omega & s+\frac{R}{L} \end{bmatrix}^{-1} \times \begin{bmatrix} \frac{1}{L} & 0 \\ 0 & \frac{1}{L} \end{bmatrix} \tag{28}$$

9. G^u_{pll} is the phase-locked loop model 2, which is used to characterize the disturbance included in the output angle of the phase-locked loop caused by the grid voltage disturbance, which in turn causes calculation error for the voltage in d-axis and q-axis.

$$G^u_{pll} = \begin{bmatrix} 0 & -U_q \times \dfrac{G_{PI-PLL}}{s+U_{gd}\times G_{PI-PLL}} \\ 0 & U_d \times \dfrac{G_{PI-PLL}}{s+U_{gd}\times G_{PI-PLL}} \end{bmatrix} \tag{29}$$

where U_d represents the steady-state value of d-axis output voltage u_d, and U_q represents the steady-state value of q-axis output voltage u_q.

10. The transfer function $G_{p\text{-}u}$ is used to characterize the mathematical relationship between the output power P_{dc} of the DC bus in the battery energy storage converter and the small signal disturbance of the grid voltage. The specific expression is:

$$G_{P\to u}=\begin{bmatrix}\frac{3}{2}I_d & \frac{3}{2}I_q\end{bmatrix} \tag{30}$$

11. The transfer function $G_{p\text{-}i}$ is used to characterize the mathematical relationship between the output power P_{dc} of DC bus in the battery energy storage converter and the small-signal disturbance of the grid current.

$$G_{P\to i}=\begin{bmatrix}\frac{3}{2}U_{gd}+\frac{3}{2}LI_d s & \frac{3}{2}LI_q s\end{bmatrix} \tag{31}$$

12. The transfer function $G_{Pg\text{-}u}$ is used to characterize the mathematical relationship between the grid-side output power P_g of the battery energy storage converter and the small-signal disturbance of the grid voltage. Its specific expression is:

$$G_{Pg-u}=\begin{bmatrix}\frac{3}{2}I_d & \frac{3}{2}I_q\end{bmatrix} \tag{32}$$

13. The transfer function $G_{P\text{-}\varphi}$ is used to characterize the mathematical relationship between the small-signal disturbance of the power P_{DAB} on the DAB side and the small-signal disturbance of the phase-shift angle. The specific expression is as follows:

$$G_{P\to\varphi}=\begin{cases}\dfrac{U_{dc0}U_{BAT}\left(\pi-2\varphi_0\right)}{2N\pi^2 f_{s1}L_{DAB}} & \varphi_0\geq 0\\ \dfrac{U_{dc0}U_{BAT}\left(\pi+2\varphi_0\right)}{2N\pi^2 f_{s1}L_{DAB}} & \varphi_0<0\end{cases} \tag{33}$$

where φ_0 represents the phase shift angle under steady-state conditions, meanwhile U_{dc0} represents the DC bus voltage under steady-state conditions.

14. $G_{PI\text{-}DAB}$ is the PI regulator in active power loop. The specific expression of $G_{PI\text{-}DAB}$ is:

$$G_{PI-DAB}=k_{pDAB}+\frac{k_{iDAB}}{s} \tag{34}$$

where k_{pDAB} and k_{iDAB} represent the proportional and integral coefficients of the PI regulator in active power control loop, respectively.

15. P_{ref} is the small-signal perturbation for a given value of active power. The reference value of active power is a constant in steady state, so this term can be regarded as zero.

16. The transfer function $G_{Pg\text{-}i}$ is used to characterize the mathematical relationship between the grid-side output power P_g of the battery energy storage converter and the small-signal disturbance of the grid current.

$$G_{Pg-i}=\begin{bmatrix}\frac{3}{2}U_{gd} & \frac{3}{2}U_{gq}\end{bmatrix} \tag{35}$$

where U_{gd} represents the steady-state value of grid voltage in d-axis, and U_{gq} represents the steady-state value of grid voltage in q-axis.

17. G_{dc} is the transfer function of the capacitance in DC bus, which is expressed as:

$$G_{dc}=\frac{1}{sCU_{dc0}} \tag{36}$$

18. G_{DAB2} represents the effect of small signal disturbance included in DC voltage on DAB output power. The specific expression is as follows:

$$G_{DAB2}=\frac{U_B\varphi_0\left(\pi-\left|\varphi_0\right|\right)}{2\pi^2 f_s L_s}\times\tilde{u}_{dc} \tag{37}$$

To sum up, after simplifying the block diagram, the relationship between u_{gdq} and i_{gdq} can be obtained as:

$$\begin{aligned}&(G_1G_{P-\varphi}G_{PI-DAB}G_{Pg-u}+G_1G_{P\to u}\\&-G_{VSC}G_{PI-C}G^i_{PLL}+G_{VSC}G_{DE}G^i_{PLL}\\&+G_{VSC}G^u_{PLL}-I_{2\times2})\tilde{u}_{gdq}\\&=(G_0^{-1}-G_1G_{P-\varphi}G_{PI-DAB}G_{Pg-i}\\&-G_1G_{P\to i}+G_{VSC}G_{PI-C}-G_{VSC}G_{de})\tilde{i}_{dq}\end{aligned} \tag{38}$$

Where G_1 is:

$$G_1=\frac{G_{VSC}G_{PI-C}C_{1-2}G_{PI-DC}}{sCU_{dc0}-G_{DAB2}} \tag{39}$$

According to Eq. 38 we will get:

$$\begin{aligned}Z_{out}=&(G_1G_{P-\varphi}G_{PI-DAB}G_{Pg-u}+G_1G_{P\to u}\\&-G_{VSC}G_{PI-C}G^i_{PLL}+G_{VSC}G_{de}G^i_{PLL}+G_{VSC}G^u_{PLL}\\&-I_{2\times2})^{-1}\times(G_0^{-1}-G_1G_{P-\varphi}G_{PI-DAB}G_{Pg-i}\\&-G_1G_{P\to i}+G_{VSC}G_{PI-C}-G_{VSC}G_{de})\end{aligned} \tag{40}$$

So far, the small-signal output impedance modeling of the battery energy storage converter is completed. Z_{out} is a matrix with 2 rows and 2 columns in d-q frame.

V. Simulation Result

In this section, a simulation model for a 3kW Two-stage BES-PCS based on DAB is built to validate the theoretical analysis presented in this paper using the MATLAB/Simulink environment. Besides, an example is provided to verify the correctness of the impedance model proposed in section IV.

The results of BES-PCS for discharging are shown in Fig. 8. The waveforms show that PCS starts to transmit energy from battery to the grid at 0.02s. After a short adjustment time (about half a switching cycle), the phase of currents finally synchronizes with the grid voltage which means BES-PCS operates with unity power factor. Meanwhile, the waveforms of gird current in d-q-frame and voltage of DC bus are also shown in Fig. 8(b). The

initial value of voltage is set to 400V, which can also be adjusted to steady state quickly after starting discharging. At the same time, the charging performance of BESPCS has also been verified and the result is shown in Fig. 9.

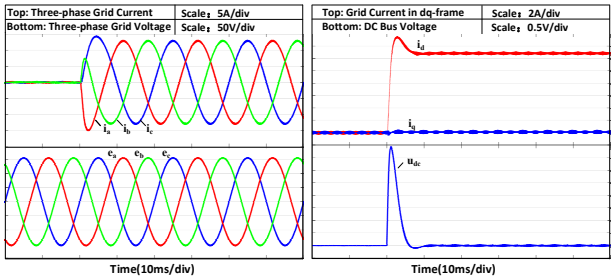

(a) (b)

Fig. 8. Start-up and steady-state operation waveforms (discharge)

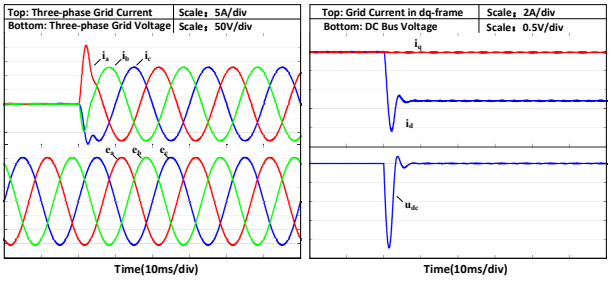

(a) (b)

Fig. 9. Start-up and steady-state operation waveforms (charge)

Fig. 10 illustrates the output power of DAB. Regardless of charging or discharging, the output power of DAB can always be regulated to its reference thanks to the power loop. The two-direction flow of energy in two-stage BES-PCS can be ensured.

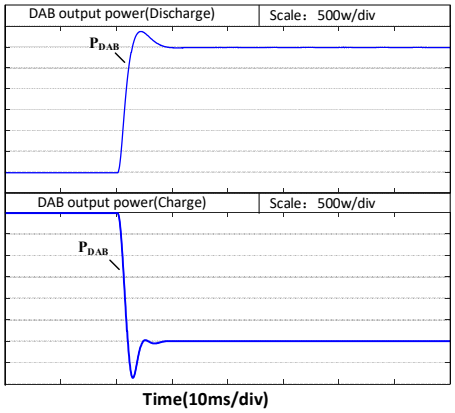

Fig.10. output power of DAB

Meanwhile, an example is used to verify the correctness of the impedance model proposed in section IV. The main parameters of the two-stage battery energy storage converter are given in Table I.

The rated power of the converter is 3kW, the rated voltage of the grid is 110V, and the rated frequency of the grid is 50Hz. The system is stable if and only if the feedback loop gain term $Z_g \times Z_{out}^{-1}$ satisfies the generalized Nyquist criterion.

When L_g=1mH (strong power grid), the Nyquist curve of $Z_g \times Z_{out}^{-1}$ and the simulation waveforms are shown in Fig. 11 and Fig. 12, respectively.

TABLE I
PARAMETER OF THE DAB-BESS

Symbol	Meaning	Value
$U_{ph\text{-}rms}$	single-phase grid voltage	110V (Effective value)
U_b	Battery Voltage	200V
U_{dc0}	DC bus voltage	400V
f_{s1}	Switching frequency of DAB	10kHz
f_{s2}	Switching frequency of Inverter	20kHz
p_g	Output Power	3kW
C_{dc}	Bus capacitance	3mH
L_s	Transformer leakage inductance of DAB	0.05mH
L_{AC}	Filter inductance	3.6mH
R_{AC}	Resistance of Filter inductor	10mΩ
N	Transformer ratio	0.5
k_{ip} /k_{ii}	PI Parameters of Current Loop	0.8/600
K_{vp}/k_{vi}	PI Parameters of Voltage Loop	0.2/0.5
k_{pDAB}/k_{iDAB}	PI Parameters of DAB Power Loop	0.2e-3/1.0e-3
k_{ppll}/k_{ipll}	PI Parameters of phase-locked loop	1/300

The Nyquist curve in Fig. 11 does not go around the point of (-1,0), which means the converter can run normally. The simulation results in Fig. 12 also confirms this conclusion, the waveforms of grid-side current is basically sinusoidal and the currents in d-q frame is basically DC.

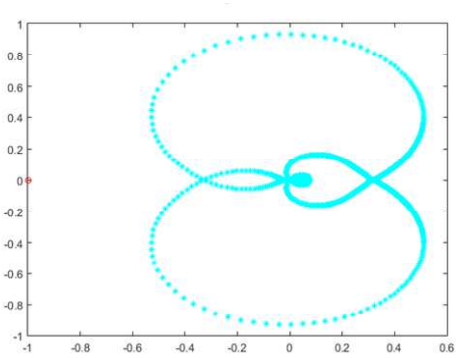

Fig. 11. Nyquist plot when Lg=1mH

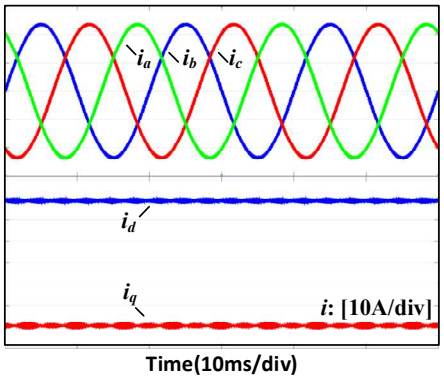

Fig. 12. Simulation waveforms in time domain when Lg=1mH

When L_g=10mH (weak power grid), the Nyquist curve of $Z_g \times Z_{out}^{-1}$ is shown in Fig. 13. It can be acknowledged from Fig. 13 that the curve wraps around the point of (-1,0) which means the system is unstable. Simulation

waveforms in this case also illustrate that the current oscillates, which are portrayed in Fig. 14. The waveforms are seriously distorted. It means system cannot operate normally with large inductance.

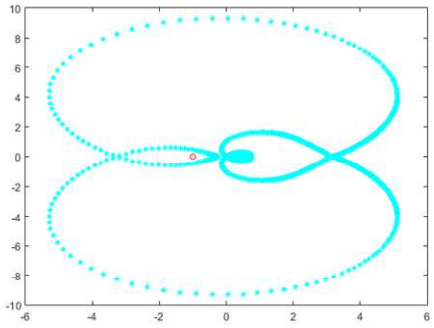

Fig. 13. Nyquist plot when Lg=15mH

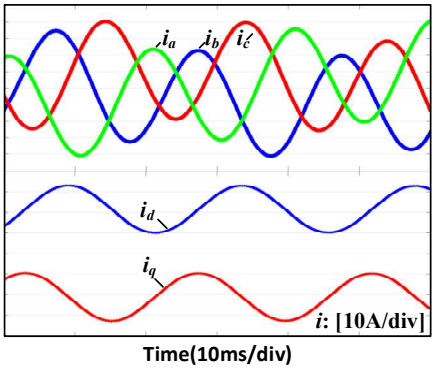

Fig. 14. Simulation waveforms in time domain when Lg=15mH

From the above analysis, it can be determined that the control loops of the BES-PCS can ensure the stable operation of the system, meanwhile, the small signal impedance modeling of the battery energy storage converter is accurate.

VI. Conclusion

This paper introduces a 110V/3kW two-stage battery energy storage power conversion system based on dual active bridge. The working principle and control strategy of its two stages are analyzed. Moreover, a small-signal output impedance model is also established to analyze the stability of the battery energy storage converter under weak grid. In the end, a corresponding simulation model is built to check the feasibility of the system and an example is provided to verify the correctness of the impedance model.

Acknowledgment

The research in this paper is supported by NSFC (No. 51907119) and Shanghai Sailing Program (No. 19YF1418700).

References

[1] X. Li, D. Hui and X. Lai, "Battery Energy Storage Station (BESS)-Based Smoothing Control of Photovoltaic (PV) and Wind Power Generation Fluctuations," in IEEE Transactions on Sustainable Energy, vol. 4, no. 2, pp. 464-473, April 2013.

[2] N. W. Miller, R. S. Zrebiec, G. Hunt and R. W. Deimerico, "Design and commissioning of a 5 MVA, 2.5 MWh battery energy storage system," Proceedings of 1996 Transmission and Distribution Conference and Exposition, 1996, pp. 339-345.

[3] N. M. L. Tan, T. Abe and H. Akagi, "Design and Performance of a Bidirectional Isolated DC–DC Converter for a Battery Energy Storage System," in IEEE Transactions on Power Electronics, vol. 27, no. 3, pp. 1237-1248, March 2012.

[4] J. Walter and R. W. De Doncker, "High-power galvanically isolated DC/DC converter topology for future automobiles," IEEE 34th Annual Conference on Power Electronics Specialist, 2003. PESC '03., 2003, pp. 27-32 vol.1.

[5] B. Zhao, Q. Song, W. Liu and Y. Sun, "Overview of Dual-Active-Bridge Isolated Bidirectional DC–DC Converter for High-Frequency-Link Power-Conversion System," in IEEE Transactions on Power Electronics, vol. 29, no. 8, pp. 4091-4106, Aug. 2014.

[6] C. Wang and Q. Song, "The Research on the Triple Phase Shift Control of the Isolated Bidirectional DC-DC Converter," 2019 IEEE 3rd International Electrical and Energy Conference (CIEEC), 2019, pp. 1-6.

[7] C. Mi, H. Bai, C. Wang, and S. Gargies. Operation, design and control of dual H-bridge-based isolated bidirectional dc-dc converter [J]. IET Power Electron, 2008, 1(4): 507-517.

[8] X. Chen, W. Wu, N. Gao, H. S. -H. Chung, M. Liserre and F. Blaabjerg, "Finite Control Set Model Predictive Control for LCL-Filtered Grid-Tied Inverter With Minimum Sensors," in IEEE Transactions on Industrial Electronics, vol. 67, no. 12, pp. 9980-9990, Dec. 2020, doi: 10.1109/TIE.2019.2962444.

[9] N. Gao, B. Zhang, W. Wu and F. Blaabjerg, "Finite control set model predictive control integrated with disturbance observer for battery energy storage power conversion system," Journal of Power Electronics, vol. 21, no. 2, pp. 342-353, 2021. DOI: 10.1007/s43236-020-00197-2.

[10] F. Deng, J. Zhao, C. Liu, Z. Wang, X. Cai and F. Blaabjerg, "Temperature-Balancing Control for Modular Multilevel Converters Under Unbalanced Grid Voltages," in IEEE Transactions on Power Electronics, vol. 37, no. 4, pp. 4614-4625, April 2022, doi: 10.1109/TPEL.2021.3123634.

[11] S. Inoue and H. Akagi, "A Bidirectional DC–DC Converter for an Energy Storage System With Galvanic Isolation," in IEEE Transactions on Power Electronics, vol. 22, no. 6, pp. 2299-2306, Nov. 2007.

[12] N. Gao, Q. Chen, R. Li and X. Cai, "Multi-level cascaded medium frequency isolated power conversion system based on dual active bridge," 2014 International Power Electronics and Application Conference and Exposition, 2014, pp. 1045-1048.

[13] B. Zhao, Q. Song, W. Liu and Y. Sun, "A Synthetic Discrete Design Methodology of High-Frequency Isolated Bidirectional DC/DC Converter for Grid-Connected Battery Energy Storage System Using Advanced Components," in IEEE Transactions on Industrial Electronics, vol. 61, no. 10, pp. 5402-5410, Oct. 2014, doi: 10.1109/TIE.2014.2304915.

[14] J. Sun and K. J. Karimi, "Small-signal input impedance modeling of line-frequency rectifiers," in IEEE Transactions on Aerospace and Electronic Systems, vol. 44, no. 4, pp. 1489-1497, Oct. 2008, doi: 10.1109/TAES.2008.4667724.

[15] B. Wen, D. Dong, D. Boroyevich, R. Burgos, P. Mattavelli and Z. Shen, "Impedance-Based Analysis of Grid-Synchronization Stability for Three-Phase Paralleled Converters," in IEEE Transactions on Power Electronics, vol. 31, no. 1, pp. 26-38, Jan. 2016, doi: 10.1109/TPEL.2015.2419712.